Eutectic colony formation in systems with interfacial energy anisotropy: A phase field study

Arka Lahiri[a,*], Chandrashekhar Tiwary[a], Kamanio Chattopadhyay[a], Abhik Choudhury[a]

[a]*Department of Materials Engineering, Indian Institute of Science, Bangalore - 560 012, India.*

arXiv:1607.02722v3 [cond-mat.mtrl-sci] 11 Dec 2016

Abstract

Instability of a binary eutectic solidification front to morphological perturbations due to rejection of a ternary impurity leads to the formation of eutectic colonies. Whereas, the instability dynamics and the resultant microstructural features are reasonably well understood for isotropic systems, several experimental observations point to the existence of colonies in systems with anisotropic interfaces. In this study, we extend the understanding of eutectic colonies to anisotropic systems, where certain orientations of the solid-liquid or solid-solid interfaces are associated with a lower free energy than the others. Through phase field simulations in 2D and 3D, we have systematically probed the colony formation dynamics and the resulting microstructures, as functions of the pulling velocity and the relative orientation of the equilibrium interfaces with that of the imposed temperature gradient. We find that in 2D, stabler finger spacings are selected with an increase in the magnitude of anisotropy introduced, either in the solid-liquid or in the solid-solid interface. The fingers have a well-defined orientation for the case of anisotropy in the solid-liquid interface, with no fixed orientations for the lamellae constituting the colony. For the case where anisotropy exists in the solid-solid interface, the lamellae tend to orient themselves along the direction of the imposed temperature gradient, with tilted solid-liquid interfaces from the horizontal. The 3D simulations reveal existence of eutectic spirals which might become tilted under certain orientations of the equilibrium interfaces. Our simulations are able to explain several key features observed in our experimental studies of solidification in Ni-Al-Zr alloy.

Keywords: Phase-field; Mullins-Sekerka; multi-component; eutectic; colonies; anisotropy

1. Introduction

Two-phase growth in a ternary alloy where the two phases exchange two components and reject an impurity into the liquid, results in the formation of a boundary layer of this component ahead of the solidification front. This interface is then unstable to morphological perturbations much in the same manner as in a Mullins-Sekerka instability [1] (henceforth will be referred to as MS instability) of the solidification front during single phase growth. The amplification of these instabilities leads to the formation of eutectic colonies (also called two-phase fingers) which are cells made up of two-phase lamellae.

Experimentally, eutectic colonies have been extensively studied, as in [2, 3, 4, 5, 6, 7, 8]. including a study on their dynamics during directional solidification of thin samples [9]. Furthermore, Akamatsu et al. [10] are the first to observe and characterize the helical arrangement of two eutectic solids about a finger axis, which they anoint as "eutectic spirals" . They also point out the presence of

*Corresponding author

Email addresses: arka@platinum.materials.iisc.ernet.in (Arka Lahiri), cst311@gmail.com (Chandrashekhar Tiwary), kamanio@materials.iisc.ernet.in (Kamanio Chattopadhyay), abhiknc@materials.iisc.ernet.in (Abhik Choudhury)

such structures in studies that predate their observation, like the one in Al-Cr-Nb systems carried out by Souza et al. [11].

Theoretical understanding of this problem begin with the study by Plapp and Karma [12], where they perform linear stability analysis to establish that the instability leading to colony formation is oscillatory compared to the one operating on a single phase binary solid-liquid interface. The experimental observation that a spiral tip radius (ρ) scales linearly with the lamellar width (λ) [10] leads to an analytical establishment of the scaling of ρ with $V^{-0.5}$, where V is the spiraling dendrite tip growth velocity [13].

Numerical computations performed to study eutectic colony formation dynamics augment theoretical understanding in regimes outside the purview of linear analysis. In this regard, phase field simulations of eutectic colonies by Plapp and Karma [14] not only validate their theory in [12], but also highlight the lack of a stable cellular morphology under isotropic conditions.

While the studies in the previous cases concentrate on isotropic eutectics, alloys systems in general contain phases which either have anisotropic solid-liquid interfaces or where the interfacial boundaries between the solid phases have a preferred alignment of crystallographic planes giving rise to defined orientation relationships for these interfaces. Experimentally, anisotropic interfacial energies of the solid-solid interfaces have been found to result in spirals in binary eutectic alloys [15, 16].

Ni-Al-Zr is another exemplary system consisting of two solid intermetallic phases (Ni_3Al and Ni_7Zr_2) whose crystallographic planes share a well defined orientation relationship as revealed by the TEM diffraction patterns in Fig. 1(a) and 1(b). The two-phase eutectic in this alloy is also a monovariant reaction and is therefore unstable to morphological perturbations. Detailed characterization of the colonies shows that the central stem of the colonies have well aligned lamellar feature as seen in Fig. 1(c). Further resolution of the colony microstructures at the interface between two colonies reveals features resembling spiraling of two solid phases.

The influence of a well defined orientation relationship between the eutectic solids in a binary system on its steady-state growth morphologies has been studied theoretically, numerically and experimentally in [17, 18, 19]. Pusztai et al. [20] and Ratkai et al. [21], investigate the influence of kinetic anisotropy in stabilizing the spiral microstructures during two-phase eutectic colony formation in a ternary alloy by conducting phase field simulations. However, no studies exist which systematically investigate the influence of anisotropy in the interfacial energies on the colony morphology arising out of the destabilization of steady-state two-phase growth interface, in either thin-film geometry or during bulk solidification.

This motivates the two principal aims in our paper. Firstly, we perform phase field simulations to investigate the influence of the anisotropy of the different interphase interfaces on eutectic colony morphologies in thin-film geometry. Secondly, through phase-field simulations in three-dimensions we characterize the influence of anisotropy both in the solid-solid and solid-liquid interfaces on the morphologies of the spirals and the colony structures.

In what follows, we perform phase-field simulations of the following directionally solidifying systems: one where the interfacial energy is isotropic, followed by systems with anisotropic solid-liquid and solid-solid interfacial energies in 2D. Our simulations in this regard can be thought to be representative of the solidification experiments carried out for thin samples [9]. The colony formation dynamics and the resultant lamellar morphologies for each of these situations are studied as functions of the anisotropy strength and the sample pulling velocity.

We also perform 3D simulations in order to understand the effect of an introduction of a third dimension on the lamellar structures in directionally solidified systems with anisotropic solid-liquid and solid-solid interfacial energies. Our simulations are numerical studies of the eutectic spi-

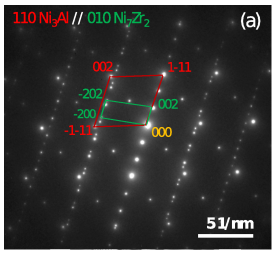

(a)

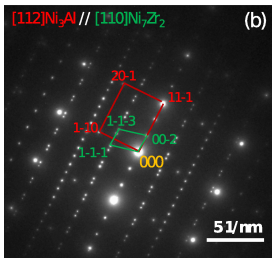

(b)

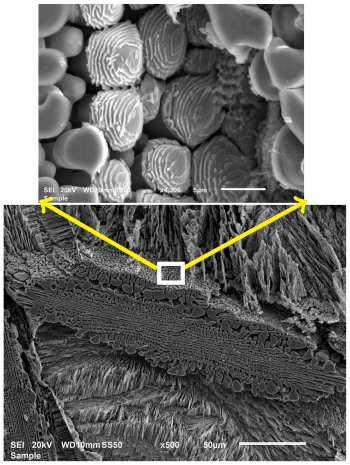

(c)

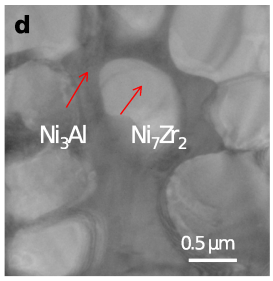

(d)

Figure 1: The anisotropy in solid–solid interfacial energy is indicated by the existence of a well defined orientation relationship between the two phases in (a) and (b). The orientation of the lamellae along the axis of the colony finger along with some spiral like features is displayed in (c). The two eutectic phases are identified from their contrast in (d).

raling observed experimentally in [10]. The computational cost involved in these simulations restricts us to a single choice in both the pulling velocity and the strength of anisotropy.

We begin with a discussion of 2D isotropic systems.

2. 2D: Isotropic system

We begin our discussion with the isotropic system where we briefly review the mathematical model developed by Plapp and Karma [14]. The colony formation dynamics and the resulting lamellar and cellular morphologies are also discussed here.

2.1. Phase-field model

The two independent components chosen to describe the ternary system are u and $\tilde{c}$: u participates in the eutectic reaction by being redistributed between the two eutectic solids and $\tilde{c}$ is partitioned equally between either of the eutectic solids and the liquid phase (K being the equilibrium partition coefficient) to set up the Mullins-Sekerka (MS) instability [1] during directional growth. The solid and liquid free energy densities are given by:

$$f_{sol} = \frac{1}{8}(u^2-1)^2 + (\tilde{c}\ln\tilde{c} - \tilde{c}) - (\ln K)\tilde{c} - \frac{\Delta T}{T_E}, \qquad (1)$$
$$f_{liq} = \frac{1}{2}u^2 + (\tilde{c}\ln\tilde{c} - \tilde{c}),$$

where $\Delta T/T_E = (T - T_E)/T_E$ is the scaled and non-dimensionalized undercooling in the system with T_E and T denoting the non-dimensional eutectic temperature and the temperature field in the system, respectively. The equilibrium values of u and $\tilde{c}$ in the solid and the liquid phases (i.e., u_s, u_l, $\tilde{c_s}$ and $\tilde{c_l}$) are computed by solving for a set of equations mentioned in the Appendix.

For the u field, solving for the equilibrium phase compositions yield $u_s = \pm 1$ and $u_l = 0$. This allows identification of the eutectic solids with the solid phase corresponding to $u_s = 1$ named α and the one corresponding to $u_s = -1$ called β.

The temperature profile (T) in the Bridgman furnace is given by:

$$T = T_0 + G(z - Vt), \tag{2}$$

where G is the imposed thermal gradient along the vertically upward direction, V is the pulling velocity, t is the time and z is the distance measured in a frame attached to the solidification front at $t = 0$. The constant T_0 is calculated by setting the undercooling at the solid-liquid interface at $t = 0$ to a pre-determined value.

The free energy functional representing a solidifying system containing diffuse interfaces is given by [22, 23],

$$F = \int_V \Bigg[(h(\phi) f_{sol} + (1 - h(\phi)) f_{liq}) + \frac{W_u^2}{2} (\nabla u)^2 + \frac{W_\phi^2}{2} (\nabla \phi)^2 \Bigg] dV, \tag{3}$$

where V is the volume undergoing eutectic solidification. W_u and W_ϕ are the parameters determining the energy penalty associated with the presence of gradients in u and ϕ respectively. A liquid-to-solid phase transformation is modeled by solving the Allen-Cahn equation [24] which represents a minimization of F w.r.t the spatial variation of ϕ, where $\phi = 0$ denotes liquid and $\phi = 1$ represents the solid with values between 0 and 1 existing at the diffuse solid-liquid interface. The governing equation for ϕ evolution can be written as,

$$\tau \frac{\partial \phi}{\partial t} = W_\phi^2 \nabla^2 \phi - g'(\phi) + h'(\phi)(f_{liq} - f_{sol}), \tag{4}$$

where $'$ indicate derivatives with respect to ϕ. τ is the relaxation time for ϕ evolution. The potential barrier between the solid and the liquid phases is given by: $g(\phi) = \phi^2(1 - \phi)^2$, and the last term in the RHS of Eq. 4 represents the driving force for solidification obtained from the relative difference in the bulk free energy densities of the solid and the liquid phases with the total bulk energy density of the system at any point in space being given by:

$$f = h(\phi) f_{sol} + (1 - h(\phi)) f_{liq}, \tag{5}$$

where $h(\phi) = \phi^2(3-2\phi)$ is a polynomial interpolant ($h(\phi) = 1$ for solid and $h(\phi) = 0$ for liquid). The evolution of u and $\tilde{c}$ with time are obtained by solving the Cahn-Hilliard equation [25] as given by:

$$\frac{\partial u}{\partial t} = \nabla \cdot \left[M \nabla \left(\frac{\partial f}{\partial u} - W_u^2 \nabla^2 u \right) \right], \tag{6}$$

and,

$$\frac{\partial \widetilde{c}}{\partial t} = \nabla \cdot \left[\widetilde{M} \nabla \left(\frac{\partial f}{\partial \widetilde{c}} \right) \right]. \tag{7}$$

M and $\widetilde{M}$ are the mobilities corresponding to evolution of u and $\widetilde{c}$ respectively, which are given by,

$$\begin{aligned} M &= D\,(1 - \phi^n)\,, \\ \widetilde{M} &= \widetilde{D}\,(1 - \phi^n)\,\widetilde{c}, \end{aligned} \tag{8}$$

where D and $\widetilde{D}$ represent constants set to unity. Eq. 8 ensures that there is no diffusion of solutes inside the solid compared to that in the liquid. As the exchange of u between α and β happens only at the advancing solidification front, higher values of the constant n will be required to allow for complete solute re-distribution in simulations of directional solidification at higher pulling velocities (V).

All of the ϕ, u and $\widetilde{c}$ fields undergo changes across a solid-liquid interface: ϕ changes from 1 to 0, u changes from ± 1 to 0 and $\widetilde{c}$ from $\widetilde{c_s}$ to $\widetilde{c_l}$. So, a solid-liquid interface can be isolated from the ϕ field by identifying locations where it has values lying between 1 and 0. But across a solid-solid (α-β) interface only the u field can be seen to be varying, (i.e., it changes from 1 to -1 as we go from α to β) while ϕ and $\tilde{c}$ remain constant; this provides the only means of identifying the solid-solid interfaces.

2.2. Results

The 2D simulation of such a system (see Fig. 2) illustrates the fundamental eutectic cell formation dynamics. The introduction of some random noise at the solid-liquid interface at $t = 0$, sets up the MS-type instability through the $\tilde{c}$ component (see Fig. 2(c)).

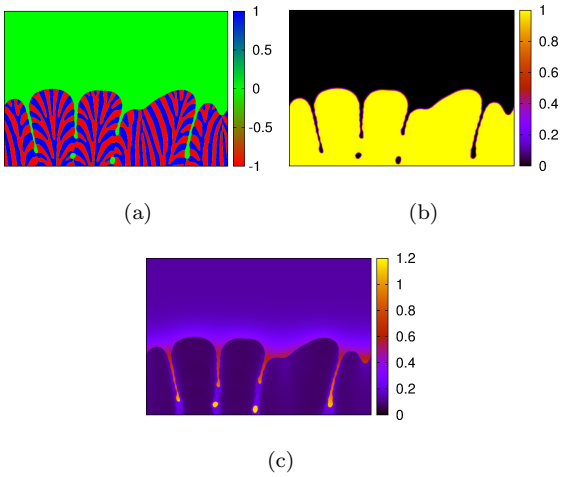

Figure 2: Colonies in an isotropic system at a total time of 150000 as seen from the (a)u field, (b)ϕ field, and (c)$\tilde{c}$ field, with no diffusivity in the solid. Colorbars report values of the u, ϕ and $\tilde{c}$ fields in (a), (b) and (c) respectively. The simulation parameters used for this study are : $G = 0.001$, $V = 0.015$, $\tau = 1.0$, $D = 1$, $\tilde{D} = 1$, $n = 4$, $dt = 0.0025$, $dx = 1$, $dy = 1$, $W_\phi = 3.2$, $W_u = 1.7$, $\tilde{c_s} = 0.025$ and $\tilde{c_l} = 0.125$. The parameter T_0 in Eq. 2 is computed by setting the initial undercooling at the solid-liquid interface to 0.1. Periodic boundary conditions are imposed at the vertical boundaries and no-flux at the horizontal ones in a simulation box of dimensions 1440 by 1000 containing 40 lamellae pairs.

The morphological instability of the solid-liquid interface leads to formation of fingers, which are identified by digit like protuberances of the solid into the liquid (see Fig. 2). Here, the system does not select a particular eutectic finger spacing and the morphological evolution of the fingers display a cyclical character. The fingers that are already formed continue to broaden and ultimately develop solid-liquid interface concavities which continue to deepen and lead to their splitting, forming new fingers. These fingers are randomly oriented with respect to the pulling direction.

Throughout the course of the simulation, lamellae can be seen to undergo either termination or broadening followed by the formation of new lamellae by spinodal decomposition. Lamellae pairs converge and ultimately terminate at locations where the solid-liquid interface is concave inwards. At locations where the solid-liquid interface is convex outwards (usually at the tip of the fingers), the eutectic phase (either α or β) present there broadens till it develops a concavity at its interface with the liquid, prompting formation of the conjugate eutectic solid phase there. It must be noted at this point, that the mechanism of lamellae broadening followed by formation of a new phase by spinodal decomposition, prevents finger splitting, which would happen with the concavity deepening without a new phase appearing ahead.

The new lamellae which come out as a result of spinodal decomposition possess a lamellar width (λ) which is different to the one selected by the criterion of minimum undercooling at the solid-liquid interface due to Jackson and Hunt [26]. Phase separation (the liquid composition $u = 0$ decomposing to give $u = \pm 1$ corresponding to the two eutectic solids) happens only at the solidification front (ϕ having values between 0 and 1) where the spinodal length scale can be determined by following the analysis in [25], considering only the double welled part of the

potential (f_{sol}) in Eq. 6 as,

$$\begin{aligned}\frac{\partial u}{\partial t} &= \nabla \cdot \left[M \nabla \left(\frac{\partial f_{sol}}{\partial u} - W_u^2 \nabla^2 u \right) \right] \\ &= \nabla \cdot \left[M \left(\frac{\partial^2 f_{sol}}{\partial u^2} \nabla u - W_u^2 \nabla \left(\nabla^2 u \right) \right) \right] \\ &= M \left[\frac{\partial^2 f_{sol}}{\partial u^2} \nabla^2 u - W_u^2 \left(\nabla^4 u \right) \right]. \end{aligned} \tag{9}$$

where we have assumed M to be a constant (but less than D) at the interface and retained only linear terms in order to obtain the last equality. An expression describing the amplification of a sinusoidal variation in $u(= u_0 + A(t)\cos\omega x)$, with time, whose evolution is governed by Eq. 9, is given by:

$$\begin{aligned} A(t) &= A_0 \exp\left[R(\omega)t\right] \\ &= A_0 \exp\left[-M\omega^2 \left(\frac{\partial^2 f_{sol}}{\partial u^2} + W_u^2 \omega^2 \right) t \right], \end{aligned} \tag{10}$$

where A and A_0 are the amplitudes at times t and $t = 0$ respectively and ω is the wavenumber of the sinusoidal variation in u. The amplification factor,
$R(\omega) = -M\omega^2 \left(\partial^2 f_{sol}/\partial u^2 + W_u^2 \omega^2 \right)$, has a maximum for a wavenumber of,

$$\omega_{max} = \sqrt{ -\frac{\dfrac{\partial^2 f_{sol}}{\partial u^2}}{2W_u^2} }, \tag{11}$$

which leads us to an expression for $\lambda_{max}^{spin} (= 2\pi/\omega_{max})$, the dominant length scale of spinodal decomposition. Using, the simulation parameters mentioned in the caption to Fig. 2, and evaluating $\partial^2 f/\partial u^2$ at $u = 0$ we retrieve $\lambda_{max}^{spin} = 21.3$. It must be noted at this point that the dominating wavelength of spinodal decomposition (λ_{max}^{spin}) is decided only by an interplay of bulk and gradient energies as can be seen from Eq. 11 and is independent of the sample pulling velocity (V).

The other important length scale in the problem is the lamellar width (λ_{JH}) corresponding to the minimum undercooling at the eutectic front, which can be obtained by evaluating the expressions in [14]. For the parameters of our study, the Gibbs-Thomson coefficient evaluates to $\Gamma = 1.38$, and the contact angles are $\theta = 23.87°$, leading to $\lambda_{JH} = 40.6$ for $V = 0.01$. Invoking the theory of marginal stability of eutectics [27], all the eutectic length scales that are smaller than λ_{JH}, disappear with time under a long wavelength perturbation of the interface, leading to an average lamellar width in the system which is larger than λ_{JH}. This conclusively establishes that the microstructural length scales in our simulations are not determined by spinodal decomposition unless at pulling velocities of $V > 0.04$ (from the scaling of λ_{JH} with $V^{-0.5}$ given by [26]). At such high velocities, λ_{JH} becomes smaller than λ_{max}^{spin} (which remains invariant with change in V) and the lamellar width set by spinodal decomposition becomes the dominating microstructural length scale in the absence of perturbations of the solid-liquid interface.

Thus in 2D, nucleation in this manner offers only a mechanism to obtain the conjugate phase at a solid-liquid concavity. This is however unrealistic given that the undercoolings are not sufficiently high for such nucleation to occur. In reality it is a 3D mechanism, where a single phase rod rotates to appear from planes in front or behind to occupy the concavity. Therefore, here we will treat this formation of the second phase as only a mechanism allowing one to maintain the scale of the simulation.

Furthermore, in Fig. 2(a), there is no specific orientation relationship between the lamellae and the direction of solidification (vertically upwards) that is selected by the system. The lamellae appear oriented roughly orthogonal to the solidification envelope (Cahn's hypothesis) close to the solid-liquid interface (set by the force balance at the triple points) and take up more random orientations inside the fingers.

By reviewing the isotropic system, we have gained an understanding of the phase-field model which we are going to build upon in order to study the implications of incorporating anisotropic solid-liquid and solid-solid interfacial energies on colony formation. The colony dynamics and morphology observed in the 2D simulations of isotropic systems also provide a reference against which we can at-

tempt to understand the effect of anisotropic interfaces on the lamellar and cellular morphologies, beginning in the next section.

3. 2D:Effect of anisotropic interfacial energies on the colony dynamics

In this section, we describe phase-field models of systems possessing anisotropic interfacial energies and attempt to understand eutectic colony dynamics from 2D simulations. We begin our discussion by considering a system with anisotropic solid-liquid interfaces and follow it up with a discussion on systems with anisotropic solid-solid interfaces.

3.1. Anisotropic solid-liquid interface

In this section we study the cellular features and lamellar orientations in the presence of anisotropic solid-liquid interfaces. We draw upon our observations for an isotropic system as a context to understand the simulation results for this situation. We begin with a description of the phase-field model.

3.1.1. Phase Field Model

A convenient way to identify the solid-liquid interface is with gradients in ϕ. So, in order to understand the effect of a solid-liquid interfacial energy anisotropy on the microstructural features obtained during directional solidification, we introduce the anisotropy through the gradient energy term in the evolution equation of the ϕ field as given by the modified Allen-Cahn equation which writes:

$$\tau\frac{\partial\phi}{\partial t} = \left(\nabla\cdot\frac{\partial}{\partial\nabla\phi}\right)a - g'(\phi) + h'(\phi)(f_{liq} - f_{sol}), \quad (12)$$

where,

$$a = \frac{1}{2}W_\phi^2 a_c^2(\theta)(\nabla\phi)^2. \quad (13)$$

The anisotropy function (a_c) is given by:

$$a_c = 1+\delta cos(4(\theta-\theta_R)) = 1-\delta\left(3-4\left(\frac{\phi^{*4}_x+\phi^{*4}_y}{(\phi^{*2}_x+\phi^{*2}_y)^2}\right)\right), \quad (14)$$

which introduces the four-fold anisotropy into the solid-liquid interfacial energy. The *'s in the above equation indicate that the derivatives (with respect to either x or y as denoted by the subscripts) are computed in the reference frame of the crystal. The crystal reference frame can be rotated by an angle θ_R to the laboratory frame and this allows us to explore different relative orientations of the equilibrium solid-liquid interfaces with respect to the sample pulling direction (which is vertically downwards). δ sets the strength of the anisotropy. Fig. 3(a) displays a_c as a function of θ (γ plot), also highlighting the effect of a rotation of a crystal frame to the laboratory frame.

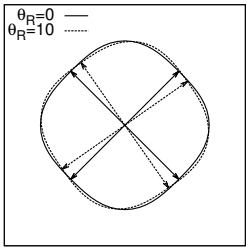

(a)

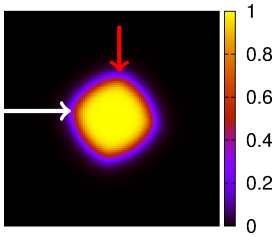

(b)

Figure 3: γ plot obtained by evaluating a_c from Eq. 14 is shown in (a). The arrows indicate the orientations of the plane normals with the least energy. Figure legends report θ_R in degrees. (b) A phase field simulation of an α nuclei growing in the liquid, with $\theta_R = 10°$, clockwise, with $\delta = 0.05$. The arrows denote the corners which can advance under directional solidification conditions. The corner identified by the red arrow dominates over the one indicated by the white one due to its closer alignment to the vertically imposed temperature gradient. Colorbar reports values from the ϕ field.

The other equations employed to model a system with anisotropic solid-liquid interfaces remain the same as reported in the isotropic situation.

3.1.2. Results

The selection of particular orientations of the solid-liquid interface under different rotations of crystal frame can also be understood by referring to Fig. 3(b).

The dynamics of colony formation in such a system is explored for a situation where the crystal frame is rotated clockwise by $\theta_R = 10^\circ$ to the laboratory frame (see Fig. 3(a)) for two different strengths of the ϕ anisotropy, i.e., $\delta = 0.015$, and 0.03, but for a single sample pulling velocity ($V = 0.015$) (see Fig. 4).

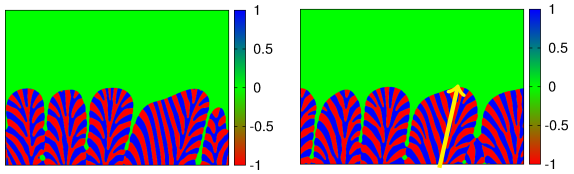

(a) (b)

Figure 4: Microstructures (u field) of a system with no solid diffusivity and solid-liquid interfacial energy anisotropy, at a total time of $t = 150000$, for (a)$\delta = 0.015$, and (b)$\delta = 0.03$, with $V = 0.015$, $n = 4$ and $\theta_R = 10^\circ$, clockwise. Colorbars report values of the u field. The other simulation parameters are the same as mentioned in the caption to Fig. 2. The arrow roughly indicates the orientation of the finger envelope.

A lot of features in these simulations are in contrast to the isotropic case. First of all, the finger envelopes tend to favor certain orientations dictated by an interplay between the anisotropy and the direction of the imposed temperature gradient (vertically upward). To illustrate this further, we can imagine that the nucleus in Fig. 3(b) being subjected to a temperature gradient prompting it to grow in the vertically upward direction. Now, the two corners (indicated by arrows) in the top half of the crystal are the ones which could grow such that the nucleus continues to be bounded by interfaces which are favored by anisotropy. But the one on the right (identified by the red arrow in Fig. 3(b)) is usually favored because of it being closer to the pulling direction. This can be clearly confirmed in Fig. 4(b) where the fingers have an orientation given by a slight clockwise rotation from the vertical (represented by the arrow in Fig. 4(b)). In situations where the solid-liquid interface is not as anisotropic (lower δ, as in Fig. 4(a)), the selection of growth direction is not as strict as in the case with higher δ (see Fig. 4(b)). This manifests as the growth of fingers along directions which are not the closest to that suggested by anisotropy under a temperature gradient. Another consequence of this is the broader appearance of fingers for $\delta = 0.015$ (Fig. 4(a)) than for $\delta = 0.03$ (Fig. 4(b)).

Also, the tilted orientation of the fingers from the vertical as observed in Fig. 4(b), during growth implies a non-zero component of their growth velocity in the horizontal direction. This leads to an observed motion of the fingers across the width of the simulation box (traveling waves of fingers) during eutectic colony growth.

Emergence of a stable finger spacing can be observed in Fig. 4(b), which is not observed in the isotropic case. In the system with lower anisotropy shown in Fig. 4(a), the fingers do broaden and bifurcate, but not as frequently as in Fig. 2, which suggests that with an increase in the magnitude of anisotropy the stability of the solid-liquid interface is enhanced.

Similar to the isotropic situation, the lamellae appear to be oriented orthogonally to the solidification envelope at the solid-liquid interface which gets modified inside the fingers due to interactions between lamellae approaching the finger axis from either side of the finger tip.

An incomplete partitioning of the solutes (also known as solute trapping) hindering the formation of the eutectic at the solid-liquid interface, is observed for higher values of V and δ when using solute mobilities of the form, $M = D\,(1-\phi^n)$ and $\widetilde{M} = \widetilde{D}\,(1-\phi^n)\,\tilde{c}$, even with higher values of n. Thus, for studying the effects of higher V and δ on the colony dynamics, we introduce another approximation in the form of equal and constant mobility of solutes in both solid and liquid phases. Mathematically, this manifests as setting $M = \widetilde{M} = 1$ in the model formulation. We report two simulations in Fig. 5 with $\delta = 0.03$ (Fig. 5(a))

and $\delta = 0.05$ (Fig. 5(b)) at a sample pulling velocity of $V = 0.04$. The enhanced solid diffusivity should lead to a λ_{JH} larger than the value computed for the system with no solid diffusivity which should prevent length scales due to spinodal decomposition becoming dominant even at higher pulling velocities of $V = 0.04$.

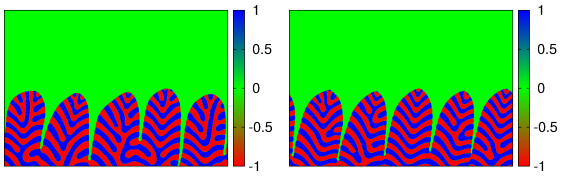

(a) (b)

Figure 5: Microstructures (u field) of a system having equal diffusivity in the solid and the liquid phases with solid-liquid interfacial energy anisotropy, for (a)$\delta = 0.03$, $t = 150000$, and (b)$\delta = 0.05$, $t = 100000$ with $V = 0.04$ and $\theta_R = 10^\circ$, clockwise. Colorbars report values of the u field. The other simulation parameters are the same as mentioned in the caption to Fig. 2.

The fingers in Fig. 5 appear to possess a smaller tip-radius than what is observed for the cells in Fig. 4, which is expected at higher velocities due to the inverse scaling of tip-radius (ρ), with pulling velocity (V) given by the constancy of $\rho^2 V$. Furthermore, an increase in δ can also be seen to promote a stronger selection of the dendrite tip radius as observed from Figs. 5(a) and 5(b). Also, the tilt of the fingers becomes more pronounced with increase in δ, as can be confirmed from Figs. 5(a) and 5(b).

An interesting difference in the lamellar appearance can be observed at the central axis of the fingers. In Fig. 4, the individual phases from the solid-liquid interface on either side of the tip of a finger do not unite at the central axis of the finger, as they do in Fig. 5. The tree-like arrangement of phases seen in Fig. 4 is not replicated in Fig. 5, where the phases from either side of the finger, join with each other in the middle of the fingers. This difference is a consequence of the lack of solute diffusivity in the solid in Fig. 4, where the local orthogonality of the lamellae to the solidification envelope remains frozen even inside the fingers, with the emanation of phases from the central stem being a record of the lamellar bifurcation that has happened earlier.

Having considered the effect of anisotropic solid-liquid interfaces on the colony dynamics, we move on to studying systems with anisotropic solid-solid interfacial energies.

3.2. Anisotropic solid-solid interface

In this section we are going to study the effect of an anisotropic interface between the two eutectic solids on the lamellar morphologies constituting the eutectic colonies and also on the orientation and stability of the fingers. We begin with a description of the phase-field model.

3.2.1. Phase-field model

In order to explore the eutectic colony formation dynamics in situations where the solid-solid (i.e., α-β) interfaces have a specific orientation with respect to the pulling direction, the anisotropy must be introduced through the u field. But considering the fact u changes in value across all the three possible interfaces (α-β, α-liquid and β-liquid), we introduce the anisotropy through the the bulk free energy density in solid, to minimize its influence on the solid-liquid interface which results in the modified free-energy density expression of the solid given by,

$$f_{sol} = \frac{1}{8}(u^2-1)^2 a_c^2(\theta) + (\tilde{c}\ln\tilde{c} - \tilde{c}) - (\ln K)\tilde{c} - \frac{\Delta T}{T_E}, \quad (15)$$

where a_c is the same as in Eq. 14 with ϕ's being replaced by u's. From Eq. 15, we can see that the free energy density contribution from the u field has a maximum at $u = 0$ and minima at $u = \pm 1$. Now by observing that the total energy density of the system is an interpolation between the solid and liquid energy densities through an interpolant(h) which is a non-linear but monotonic function of ϕ (see Eq. 5), it can be verified that at a solid-liquid interface (u varying between 0 and ± 1; ϕ varying between 0 and 1) the influence of anisotropy is mellowed down by u being non-zero and h being non-unity. To confirm this

observation, we can refer to Fig. 10 in [28]. The equilibrium orientations of the α-β interfaces under solid-solid anisotropy can be discerned from Fig. 8 in [28].

3.2.2. Results

For a given rotation of the crystal frame relative to the laboratory frame, the orientation of the α-β interface is going to be determined by the force balance at the triple points. This can be predicted for the situation of steady-state growth using symmetry arguments that are motivated from experiments [18, 19] which claim that the resultant surface tension must still be oriented along the growth direction. This condition can then be used to derive an analytical expression for the α-β interfacial orientation with the vertical [17] which we are going to henceforth refer to as the tilt angle (θ_t) (explained in Fig. 6(a)). The tilt of the solid-solid interface for a given rotation of the crystal frame can be seen in Fig. 6(a). For the four-fold anisotropy function we have implemented, we compared the tilt angles from steady-state growth simulations of a single lamella pair against theoretical predictions in Fig. 6(b).

The colony formation dynamics with anisotropic solid-solid interfacial energy is explored in Fig. 7 with two different magnitudes of anisotropy, i.e., $\delta = 0.015$ in Fig. 7(a) and $\delta = 0.03$ in Fig. 7(b) at a single pulling velocity of $V = 0.015$.

Here, the microstructural feature that is strikingly different from the previous cases of isotropy and solid-liquid anisotropy is the presence of straight, parallel, lamellae pairs running through the center of the fingers and are very similar to what is observed in Fig. 1. This qualitative agreement between our simulations and experiments substantiates our conjecture that the structures observed in Fig. 1 are a result of anisotropic interfaces and more specifically anisotropy of the interface between the two eutectic solids.

Though there is a theoretical prediction available for

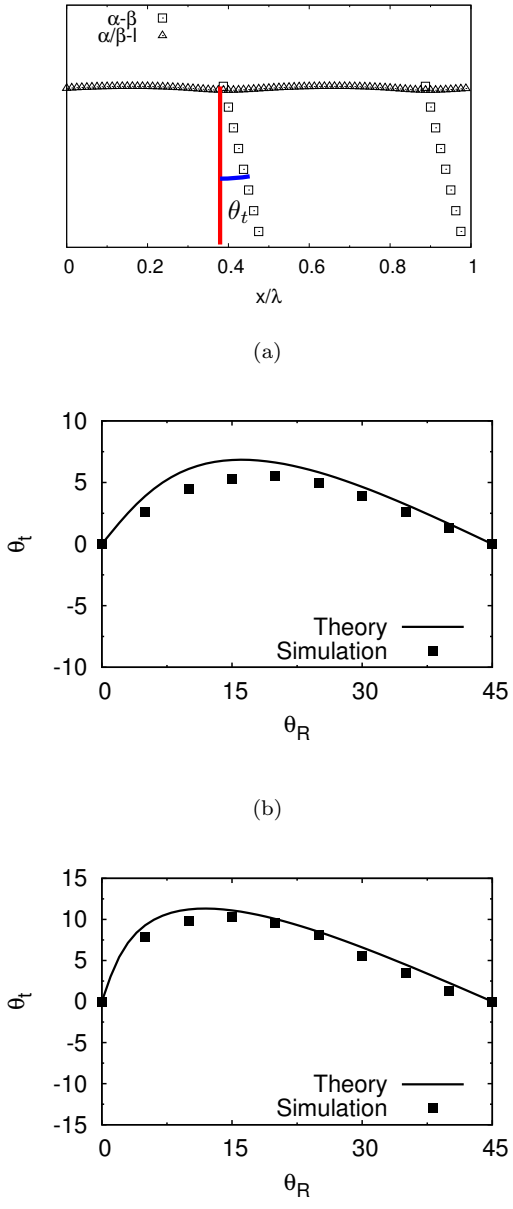

Figure 6: Tilt of the solid-solid interface for $\theta_R = 10°$, clockwise, and the corresponding tilt angle θ_t is shown in (a). Tilt angles (θ_t) are plotted versus angle between the crystal frame and the laboratory frame (θ_R), for (b) $M = \widetilde{M} = 0$, for the eutectic solids; $\delta = 0.03$, and (c) $M = \widetilde{M} = 1$ for the eutectic solids; $\delta = 0.05$.

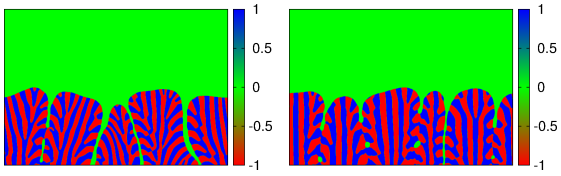

(a) (b)

Figure 7: Microstructures (u field) of a system with no solid diffusivity and solid-solid interfacial energy anisotropy, for (a)$\delta = 0.015$, $n = 16$, $t = 125000$, and (b)$\delta = 0.03$, $n = 32$, $t = 150000$, with $V = 0.015$. Colorbars report values of the u field. The other simulation parameters are the same as mentioned in the caption to Fig. 2.

the orientation of the α-β interfaces during steady-state growth, for an unsteady situation of cellular or dendritic growth we can only attempt to qualitatively understand the lamellar orientations in the absence of an analytical expression. Focusing closely on Figs. 7(a) and 7(b), the simulation proceeds from the destabilization of a tilted state of the lamellae during steady-state growth (as seen in Fig. 6(a)), giving rise to cells which globally have lamellae oriented along the direction of the temperature gradient. The solidification envelope corresponding to each cell however develops small tilts with respect to the growth direction, which can be thought of as the tilted steady state at lower velocities being rotated such that the solid-solid interfaces become aligned with temperature gradient, while the solid-liquid interface develops a tilt.

The magnitude of anisotropy also appears to play a role in lamellar orientations, as for a smaller $\delta(= 0.015)$, as seen in Fig. 7(a), the straight lamellae pairs are not strictly aligned with the vertical, whereas with $\delta = 0.03$, the lamellae display a strong alignment with the imposed temperature gradient, as can be seen from Fig. 7(b).

An outcome of the presence of lamellae oriented as closely as possible to the direction of imposed temperature gradient is the broadening of fingers, as can be clearly observed in Fig. 7(b). The shapes of the individual fingers can be understood as a result of a combined influence of the propensity of the lamellae to remain aligned with the direction of the imposed temperature gradient and that of the thermodynamically predicted relative orientations of the solid-solid and the solid-liquid interfaces under solid-solid interfacial energy anisotropy presented in Fig. 6. Thus, the vertically oriented lamellae emanate from sides of the fingers which appear roughly flat, but display a small deviation from horizontal.

Furthermore, with regards to the stability of the finger width, an increase in δ leads to stabler features, which is the same as seen for the case of anisotropic solid-liquid interfacial energy.

As mentioned in conjunction to the discussion on colony dynamics with solid-liquid anisotropy, we relax the criterion of negligible solute diffusivities in the solid in order to negate the solute-trapping that impedes probing of colony formation in systems pulled at higher velocities or displaying higher anisotropy in the interfacial energy. A variation of tilt angles (θ_t) as a function of θ_R for equal diffusivity of solutes in the solid and the liquid is also reported in Fig. 6(c) as a confirmation that this approximation preserves the ability of the model to capture the essential physics. This enables us to simulate the effects of a pulling velocity of $V = 0.04$ on systems with $\delta = 0.03$ (see Fig. 8(a)) and $\delta = 0.05$ (see Fig. 8(b)).

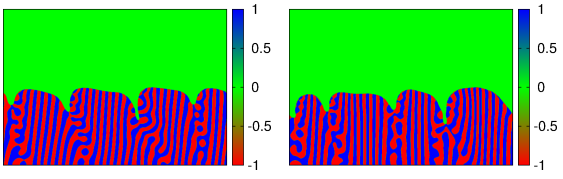

(a) (b)

Figure 8: Microstructures (u field) of a system with equal solute diffusivity in the solid and the liquid phases, with solid-solid interfacial energy anisotropy, for (a)$\delta = 0.03$; $t = 150000$ and (b)$\delta = 0.05$; $t = 150000$, with $V = 0.04$. Colorbars report values of the u field. The other simulation parameters are the same as mentioned in the caption to Fig. 2.

Most of the features seen in Fig. 7 is replicated in Fig. 8 except for a few exceptions. One of them being the absence of the deep cells observed in Fig. 7. This is a result of the

enhanced diffusivity in the solid which allows adjoining fingers to fuse wherever they are in close proximity. Another important feature of these simulations is the lateral orientation (towards the left in Fig. 8) of the two-phase finger-tips in their bid to choose a smaller tip radius (ρ) consistent with a larger pulling velocity V while allowing the maximum number of lamellae to remain vertical at the same time maintaining the necessary orientation relationship between the solid-solid and solid-liquid interfaces. Furthermore, the lamellae in Fig. 8 also appears finer consistent with the higher pulling velocities employed for these simulations [1].

Having studied the lamellar orientations and the two-phase cell morphologies for systems with anisotropic solid-solid and solid-liquid interfacial energies in 2D, we now move on to 3D simulations where we probe the effect of a third dimension on the colony dynamics in systems with anisotropic interfacial energies. We begin with a discussion of an isotropic system.

4. 3D: Isotropic

The 2D simulations provide important insights into the physics of the colony formation problem in terms of both lamellar and finger morphologies. But these observations from 2D simulations suffer from a limitation of being representative only of directional solidification in thin samples. In order to gain a complete understanding of the problem in situations where both dimensions of the solidified cross-section are comparable, we resort to 3D studies beginning with the isotropic system. The governing equations 4, 6 and 7 are expressed in a tensorial form which are numerically solved in a 3D cartesian system.

[1] λ scales as ρ with change in velocity, with the scaling constant depending on the simulation conditions. Thus, changes in lamellar widths can be understood in the context of the concurrent changes tip radius with velocity (V), which is also indicative of the magnitude of the scaling constant connecting λ and ρ for the current simulation.

The high computational cost of 3D simulations, constrain us to perform them for a set of parameters which lead to a quicker destabilization of the solidification front. Hence, we employ a high pulling velocity of $V = 0.1$ to computationally access the colony dynamics in 3D. This approach necessitates equal diffusivity of solutes in the solid to that in the liquid, due to the high solute trapping observed in this model at higher pulling speeds.

It must be mentioned at this point that though for $V = 0.1$ the spinodal decomposition length scale λ_{max}^{spin} becomes larger than λ_{JH}, the scale of the simulation in 3D is always maintained at λ_{JH} due to the presence of 3D topological mechanisms for lamellar interactions.

We report a 3D simulation in Fig. 9 carried out in a $288 \times 288 \times 300$ box containing 8 lamellae pairs along each dimension with the remaining parameters being identical to the 2D isotropic simulation shown in Fig. 5. The simulations are done in a directional solidification setting with the direction of the imposed temperature gradient being vertically upwards. The boundary conditions are set to be no-flux on faces of the box normal to the pulling direction and periodic on faces parallel to it.

In Fig. 9(c), a single lamella pair appears to construct each finger by growing continuously in a helical fashion. This structure has already been observed experimentally by Akamatsu and Faivre [10] and has been anointed by them as a "spiraling eutectic".

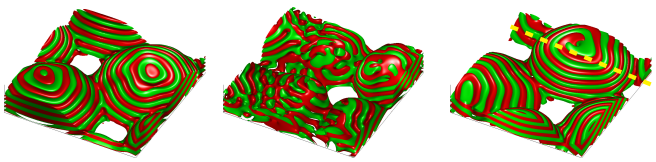

(a) (b) (c)

Figure 9: Eutectic colonies at a total time of (a)21000, (b)45000, and (c)55000 in an isotropic system with $V = 0.1$. The yellow dashed line in (c) represents the orientation of the vertical sections reported in Fig. 10.

The morphology of the spiral can be better understood by considering a 2D sections of the microstructure

in Fig. 9(c) by planes parallel and perpendicular to the growth direction as reported in Figs. 10 and 11, respectively. The apparent discontinuity in the solid phases across the central axis of the finger seen in Fig. 10(a) coupled with the particular arrangement of phases in Fig. 11 allow an understanding of the spiral as a helical arrangement of a single pair of lamella plates. Figs. 9(c), 10 and 11 considered in unison points to the possibility of the shape of the spiraling eutectic fingers being approximated by a paraboloid.

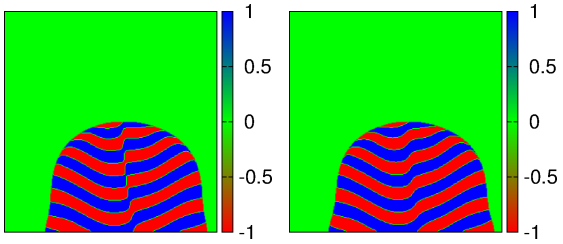

(a) (b)

Figure 10: 2D sections (u field) of Fig. 9(c) by a plane parallel to the pulling direction whose orientation is indicated by the yellow dotted line in Fig. 9(c), showing solid phase arrangements at (a)the spiral axis, and (b)a little away from the spiral axis. Colorbars report values from the u field.

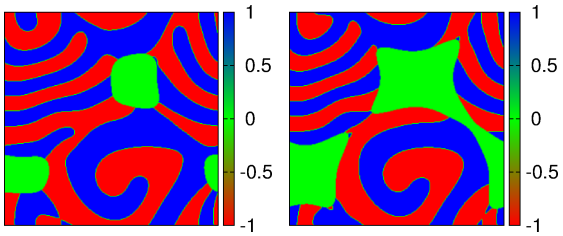

(a) (b)

Figure 11: 2D sections (u field) of Fig. 9(c) by a plane normal to the pulling direction. The sectioning height is lower in (a) than in (b). Colorbars report values from the u field.

The 3D simulation of the isotropic system confirms the major observations from the 2D simulation in terms of the randomness of the finger orientations, the lack of specificity of the lamellar orientations and the absence of a particular finger spacing selected by the same. The solid-liquid interface is found to be unstable with spirals forming and disintegrating throughout the course of the simulation as can be seen by considering the Figs. 9(a), 9(b) and 9(c).

The discussion of an isotropic system in 3D, provides a reference against which we will seek to understand the eutectic colony features under interfacial anisotropy presented in the following sections.

5. 3D: Effect of anisotropic interfacial energies on the colony dynamics

Like in 2D, we will consider the effect of both solid-liquid and solid-solid anisotropy on the colony formation dynamics in 3D. We begin with the former.

5.1. Anisotropic solid-liquid interface

To explore the effect of anisotropy on the solid-liquid interface on the colony formation dynamics in a 3D system, we introduce the anisotropy through the $\phi-$ field with the expression for a_c being:

$$a_c = 1 - \delta \left(3 - 4 \left(\frac{\phi^{*4}_x + \phi^{*4}_y + \phi^{*4}_z}{(\phi^{*2}_x + \phi^{*2}_y + \phi^{*2}_z)^2} \right) \right), \qquad (16)$$

which is a simple extension of the 2D case. In reality, the crystal frame can have any arbitrary orientation to the pulling direction. But any such orientation can be decomposed into a combination of a rotation about the pulling direction and the ones normal to it. In view of that, we can attempt to understand the microstructure formation for two basic configurations: the one where the axis of rotation of the crystal frame is the same as the pulling direction and the other where it is perpendicular. We will begin the discussion with the former.

5.1.1. Crystal frame rotated about the pulling direction

The microstructure shown in Fig. 12(b) is similar to Fig. 9(c) in terms of lamellar and finger morphologies with the influence of anisotropy showing up clearly only in the transverse section of the finger (see Fig. 14) which becomes polygonal. The longitudinal section in Fig. 13 reveals a

lamellar arrangement which is also akin to its isotropic counterpart in Fig. 10.

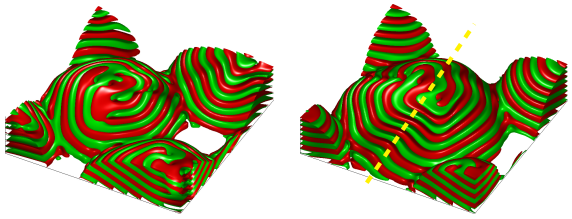

(a) (b)

Figure 12: Eutectic colonies at a total time of (a)28000, and (b)55000 in a system with solid-liquid interfacial energy anisotropy with $V = 0.1$, $\delta = 0.015$, and $\theta_R = 10°$, clockwise, about the pulling direction. The yellow dashed line in (b) represents the orientation of the vertical sections reported in Fig. 13.

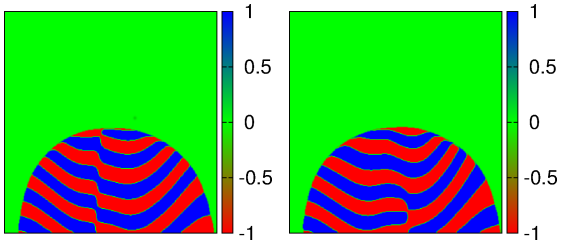

(a) (b)

Figure 13: 2D sections (u field) by a plane parallel to the pulling direction in Fig. 12(b), whose orientation is denoted by the yellow dotted line in Fig. 12(b). The section passes through and a little away from the axis of the finger in (a) and (b), respectively. Colorbars report values from the u field.

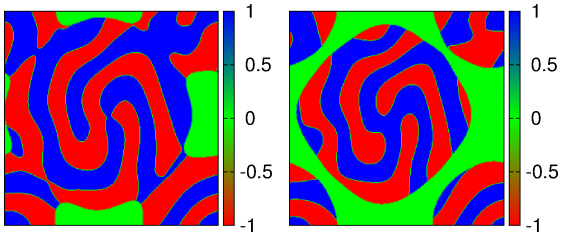

(a) (b)

Figure 14: 2D sections (u field) by a plane normal to the pulling direction in Fig. 12(b). The sectioning height is lower in (a) than in (b). Colorbars report values from the u field.

5.1.2. Crystal frame rotated about an axis normal to the pulling direction

Moving onto the situation where the reference frame of the crystal is rotated about an axis perpendicular to the direction of the imposed temperature gradient (see Fig. 15), we find fingers taking up well-defined orientations with respect to the pulling direction. The eutectic spirals in this case can be seen to be traversing the simulation box in a direction perpendicular to the pulling direction. This is due to the non-zero angle to the pulling direction taken up by the fingers while growth. Thus, the growth velocity has a lateral component which creates a traveling wave of eutectic fingers across the simulation box during growth.

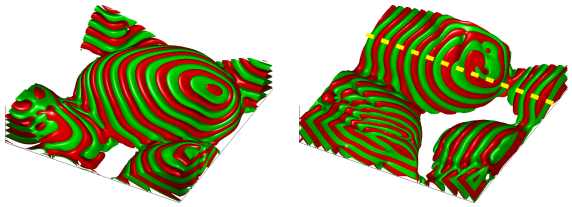

(a) (b)

Figure 15: Eutectic colonies at a total time of (a)22000, and (b)50000 in a system with solid-liquid interfacial energy anisotropy with $V = 0.1$, $\delta = 0.015$ and $\theta_R = 10°$, clockwise, about an axis normal to the pulling direction. The yellow dashed line in (b) represents the orientation of the vertical sections reported in Fig. 16.

Again, we consider sections of Fig. 15 which are parallel (Fig. 16) and normal (Fig. 17) to the pulling direction. The lack of a section which clearly demonstrates the axis as we have seen in Fig. 10(a), suggests that the finger axis is not completely contained in a single plane of such an orientation. The orientation of spirals is determined by a force balance along the tri-junction lines during its formation via the amplification of an instability, which being an unsteady phenomenon, can lead to orientations which deviate from the equilibrium orientation of interfacial planes. We can also add that, the observation of a finger axis in Fig. 10(a) is accidental and it could very well have been like the situation depicted here.

The sections in Fig. 17 are the ones which are taken to

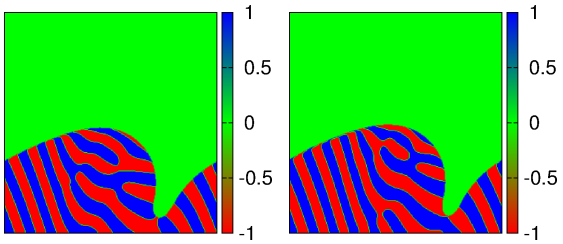

(a) (b)

Figure 16: 2D sections (u field) by a plane parallel to the pulling direction and normal to the axis of rotation of Fig. 15(b), whose orientation is denoted by the yellow dotted line in Fig. 15(b). Both figures (a) and (b) highlight that the axis of the finger is not straight. Colorbars report values from the u field.

be perpendicular to the pulling direction and parallel to the axis of rotation. Here the individual phases are either elongated or curved with the concavity towards the solid-liquid interface which is quite different to what we observe for the isotropic case in Fig. 11 and can be understood as a consequence of the tilt of the spirals.

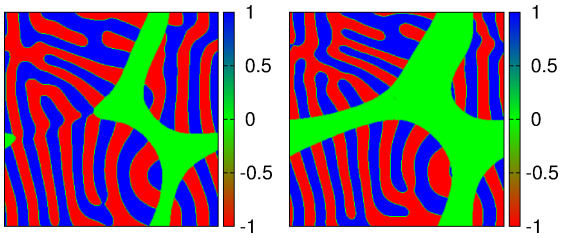

(a) (b)

Figure 17: 2D sections (u field) by a plane normal to the pulling direction and parallel to the axis of rotation of Fig. 15(b). The sectioning height is lower in (a) than in (b). Colorbars report values from the u field.

As we saw in 2D, the simulations done with an anisotropic solid-liquid interface leads to a stable finger width and orientation (see Figs. 12(a), 12(b), 15(a) and 15(b)) being selected. Thus, as opposed to the isotropic case, the spirals once formed never disintegrate, but only split when they coarsen beyond the system selected finger width.

Having understood the effect of anisotropic solid-liquid interface on the colony features in 3D, we do the same for solid-solid interfacial anisotropy in the following section.

5.2. Anisotropic solid-solid interface

The α-β interface can also have preferred orientations with respect to the direction of the imposed temperature gradient, resulting in novel patterns in the eutectic colonies. The introduction of anisotropy is done in the same way as in 2D (see Eq. 15); the anisotropy function a_c being given by Eq. 16 with u's taking the place of ϕ's.

In contrast to the stable spirals obtained for solid-liquid anisotropic interfacial energies, we do not get any spiraling for the crystal frame rotated about the pulling direction (Fig. 18(a)) and only intermittent spiraling for the situation where the crystal frame is rotated about a normal to the pulling direction (Fig. 18(b)) with the eutectic solids taking up certain well-defined orientations.

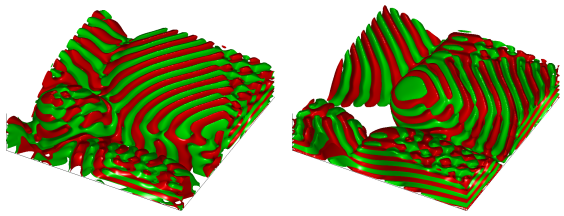

(a) (b)

Figure 18: Eutectic colonies in a system with α-β interfacial energy anisotropy with $V = 0.1$, $\delta = 0.015$ and $\theta_R = 10°$, clockwise, about, (a)the pulling direction, and (b)normal to the pulling direction.

As can be seen from Fig. 18, that the consideration of a four-fold anisotropy in the solid-solid interfacial energy leads to individual eutectic solids to arrange themselves as alternate plates which take up orientations dictated by the anisotropy. The lack of a stabilizing influence of the imposed anisotropy required for forming spirals indicates that the equilibrium interfacial orientations do not allow the formation stable spirals.

6. Summary of the results

We studied eutectic colony formation in both 2D and in 3D, in systems with preferred orientation of the solid-liquid as well as the solid-solid (α-β) interfaces. The 2D simulations with anisotropic solid-liquid interfacial energy dis-

play a stable finger spacing which has a definite orientation to the pulling direction decided by the imposed temperature gradient from the possibilities offered by equilibrium orientations of the solid-liquid interface under anisotropy. The stability of finger spacing is a function of the magnitude of anisotropy (δ), with the system selecting a well defined finger width and tip radius only at higher δ. Higher values of δ also lead to a selection of a more pronounced orientation of the fingers with respect to the pulling direction. These observations stand in stark contrast to the isotropic simulation in 2D where neither a stable finger spacing nor a well-defined orientation is taken up by the fingers. At the solidification envelope, the lamellae are oriented normal to the solid-liquid interface (also observed in the isotropic case), with no specific orientation at the center of the fingers. The effect of a higher pulling velocity (V) on the simulations is to modify the length scales manifesting as smaller lamellar width and tip radius.

When studying 2D systems with anisotropic solid-solid (α-β) interfaces, we find a significant portion of the lamellae to assume vertical or near-vertical orientations in conjunction with a slight tilt of the solid-liquid interface from the horizontal. As a consequence of this, the fingers appear much broader than what is seen for the isotropic and solid-liquid anisotropy case. With increase in δ, the lamellae appear to favor the vertical orientation strongly, as more and more of them take up such orientations. Higher pulling velocities V, resulted in finer length scales in accordance to our observation in the solid-liquid anisotropy case.

Though eutectic spirals are observed in 3D isotropic simulations, they are not stable. The existing spirals disintegrate while new ones come into existence with this process repeating throughout the course of the simulation.

The 3D simulations performed with anisotropic solid-liquid interfaces, with the crystal frame rotated about the pulling direction, revealed spirals similar to the isotropic case with the solidification envelope appearing angular. While another study done with the crystal frame rotated about an axis normal to the pulling direction led to tilted spirals. A stable finger width is selected in both the simulations.

The introduction of anisotropy in the solid-solid (α-β) interfaces lead to unstable fingers in the simulations. The rotation of the crystal frame about the pulling direction does not create spirals, rather we find elongated lamellae along particular directions normal to the vertical, which modifies to form unstable spirals when the crystal frame is rotated about an axis normal to the pulling direction.

Our 2D simulations with solid-solid anisotropy have offered a possible explanation for the existence of lamellae oriented along the finger axis in Fig. 1. Through our 3D simulations, we are able to delineate the features of eutectic spirals [10] for anisotropic solid-liquid and solid-solid interfaces. Anisotropic solid-liquid interfaces lead to the formation of stable spirals while the choice of solid-solid anisotropy leads to unstable structures occasionally resembling spirals.

7. Conclusions

We have attempted to understand pattern formation in eutectics in the presence of a ternary impurity under conditions of solid-liquid and solid-solid anisotropy. Here, through 2D simulations, we have tried to understand the effect of pulling velocity (V) and magnitude of the anisotropy (δ) on the eutectic colony microstructures for a single given rotation of the crystal frame with respect to the laboratory frame (θ_R). The patterns possible for other θ_R's under different values of V remain unexplored. The 3D simulations are carried out at a single value of both θ_R and V. The existence of novel microstructures at other combinations of these two parameters cannot be ruled out and stands as a promising area for further study. Furthermore, the absence of a stable spiral in 3D when considering solid-solid anisotropy, prompts a closer look at spiral formation and

conditions which allow or impede spiraling. Experimental studies of colony formation in anisotropic systems are critical to this end which will serve as a guide for choosing appropriate anisotropy functions in models.

Though we have been able to present and understand a lot of features of eutectic colonies for anisotropic solid-liquid and solid-solid interfaces in this study, the high solute trapping encountered for higher values of δ and V in this model point towards the possibility of employing classic solidification models [29, 30] for studying this problem to obviate this difficulty. This remains part of our future plans.

8. Acknowledgements

We are grateful to Prof. Mathis Plapp, Ecole Polytechnique, for all the insightful and critical discussions and thank him for his support.

9. Appendix

9.1. Equilibrium compositions of the phases

Solving the following set of non-linear equations yields the equilibrium compositions u_s, u_l, $\tilde{c_s}$ and $\tilde{c_l}$,

$$\begin{aligned}
&\frac{\partial f_{sol}}{\partial u}\Big|_{u_s} = \frac{\partial f_{liq}}{\partial u}\Big|_{u_l},\\
&\frac{\partial f_{sol}}{\partial \tilde{c}}\Big|_{\tilde{c_s}} = \frac{\partial f_{liq}}{\partial \tilde{c}}\Big|_{\tilde{c_l}},\\
&f_{sol} - \frac{\partial f_{sol}}{\partial u}\Big|_{u_s} u_s - \frac{\partial f_{sol}}{\partial \tilde{c}}\Big|_{\tilde{c_s}} \tilde{c_s}\\
&= f_{liq} - \frac{\partial f_{liq}}{\partial u}\Big|_{u_l} u_l - \frac{\partial f_{liq}}{\partial \tilde{c}}\Big|_{\tilde{c_l}} \tilde{c_l}. \qquad (17)
\end{aligned}$$

Eqs. 17 represent the equality of chemical potentials of u and $\tilde{c}$ with an equality of grand potentials of the two phases as the third criterion of equilibrium.

References

[1] W. W. Mullins, R. Sekerka, Stability of a planar interface during solidification of a dilute binary alloy, Journal of applied physics 35 (2) (1964) 444–451.

[2] J. Chilton, W. Winegard, Solidification of a eutectic made from zone-refined lead and tin, Journal of the Institute of Metals 89 (5) (1961) 162–164.

[3] R. Kraft, D. Albright, Microstructure of unidirectionally solidified al-cual2 eutectic, Transactions of the Metallurgical Society of AIME 221 (1) (1961) 95–102.

[4] J. Hunt, K. Jackson, Binary eutectic solidification, Transactions of the Metallurgical Society of AIME 236 (6) (1966) 843.

[5] W. Rumball, Cellular growth in eutectic systems, Metallurgia 78 (468) (1968) 141–145.

[6] P. K. Rohatgi, C. ADAMS, Colony and dendritic structures produced on solidification of eutectic aluminum copper alloy, TRANS MET SOC AIME 245 (7) (1969) 1609–1613.

[7] J. Bullock, C. Simpson, J. Eady, W. Winegard, Cell formation as the result of adding cd or sb to the pb-sn eutectic, J INST METALS, JULY 1971, 99, 212-214.

[8] M. Rinaldi, R. Sharp, M. Flemings, Growth of ternary composites from the melt: Part ii, Metallurgical Transactions 3 (12) (1972) 3139–3148.

[9] S. Akamatsu, G. Faivre, Traveling waves, two-phase fingers, and eutectic colonies in thin-sample directional solidification of a ternary eutectic alloy, Physical Review E 61 (4) (2000) 3757.

[10] S. Akamatsu, M. Perrut, S. Bottin-Rousseau, G. Faivre, Spiral two-phase dendrites, Physical review letters 104 (5) (2010) 056101.

[11] S. Souza, C. Rios, A. Coelho, P. Ferrandini, S. Gama, R. Caram, Growth and morphological characterization of al–cr–nb eutectic alloys, Journal of alloys and compounds 402 (1) (2005) 156–161.

[12] M. Plapp, A. Karma, Eutectic colony formation: A stability analysis, Physical Review E 60 (6) (1999) 6865.

[13] S. Akamatsu, S. Bottin-Rousseau, G. Faivre, E. A. Brener, Scaling theory of two-phase dendritic growth in undercooled ternary melts, Physical review letters 112 (10) (2014) 105502.

[14] M. Plapp, A. Karma, Eutectic colony formation: A phase-field study, Physical Review E 66 (6) (2002) 061608.

[15] R. Fullman, D. Wood, Origin of spiral eutectic structures, Acta Metallurgica 2 (2) (1954) 188191–189193.

[16] H. Liu, H. Jones, Solidification microstructure selection and characteristics in the zinc-based zn-mg system, Acta metallurgica et materialia 40 (2) (1992) 229–239.

[17] S. Ghosh, A. Choudhury, M. Plapp, S. Bottin-Rousseau, G. Faivre, S. Akamatsu, Interphase anisotropy effects on lamellar eutectics: A numerical study, Physical Review E 91 (2) (2015) 022407.

[18] S. Akamatsu, S. Bottin-Rousseau, M. Şerefoğlu, G. Faivre, A theory of thin lamellar eutectic growth with anisotropic interphase boundaries, Acta Materialia 60 (6) (2012) 3199–3205.

[19] S. Akamatsu, S. Bottin-Rousseau, M. Şerefoğlu, G. Faivre,

Lamellar eutectic growth with anisotropic interphase boundaries: Experimental study using the rotating directional solidification method, Acta Materialia 60 (6) (2012) 3206–3214.

[20] T. Pusztai, L. Rátkai, A. Szállás, L. Gránásy, Spiraling eutectic dendrites, Physical Review E 87 (3) (2013) 032401.

[21] L. Rátkai, A. Szállás, T. Pusztai, T. Mohri, L. Gránásy, Ternary eutectic dendrites: Pattern formation and scaling properties, The Journal of chemical physics 142 (15) (2015) 154501.

[22] J. W. Cahn, J. E. Hilliard, Free energy of a nonuniform system. i. interfacial free energy, The Journal of chemical physics 28 (2) (1958) 258–267.

[23] A. Karma, Phase-field model of eutectic growth, Physical Review E 49 (3) (1994) 2245.

[24] S. M. Allen, J. W. Cahn, A microscopic theory for antiphase boundary motion and its application to antiphase domain coarsening, Acta Metallurgica 27 (6) (1979) 1085–1095.

[25] J. W. Cahn, On spinodal decomposition, Acta metallurgica 9 (9) (1961) 795–801.

[26] K. Jackson, J. Hunt, Lamellar and rod eutectic growth, AIME Met Soc Trans 236 (1966) 1129–1142.

[27] J. Langer, Eutectic solidification and marginal stability, Physical Review Letters 44 (15) (1980) 1023.

[28] A. Lahiri, A. Choudhury, Effect of surface energy anisotropy on the stability of growth fronts in multiphase alloys, Transactions of the Indian Institute of Metals 68 (6) (2015) 1053–1057.

[29] R. Folch, M. Plapp, Quantitative phase-field modeling of two-phase growth, Physical Review E 72 (1) (2005) 011602.

[30] A. Choudhury, B. Nestler, Phys.Rev.E 85 (2011) 021602.